

TOOLS FOR COMPUTING THE AGN FEEDBACK: RADIO-LOUDNESS DISTRIBUTION AND THE KINETIC LUMINOSITY FUNCTION

F. LA FRANCA¹, G. MELINI¹ AND F. FIORE²

¹ DIPARTIMENTO DI FISICA, UNIVERSITÀ ROMA TRE, VIA DELLA VASCA NAVALE 84, I-00146 ROMA, ITALY
 EMAIL: lafranca@fis.uniroma3.it, melini@fis.uniroma3.it

² INAF-OSSERVATORIO ASTRONOMICOMI DI ROMA, VIA FRASCATI 33, I-00040, MONTEPORZIO CATONE, ITALY

Received 2009 December 30; Accepted 2010 May 27

ABSTRACT

We studied the Active Galactic Nuclei (AGN) radio emission from a compilation of hard X-ray selected samples, all observed in the 1.4 GHz band. A total of more than 1600 AGN with 2-10 keV de-absorbed luminosities higher than 10^{42} erg s⁻¹ cm⁻² were used.

For a sub-sample of about 50 $z \lesssim 0.1$ AGN it was possible to reach a $\sim 80\%$ fraction of radio detections and therefore, for the first time, it was possible to almost completely measure the probability distribution function of the ratio between the radio and the X-ray luminosity $R_X = \log(L_{1.4}/L_X)$, where $L_{1.4}/L_X = \nu L_\nu(1.4 \text{ GHz})/L_X(2-10 \text{ keV})$. The probability distribution function of R_X was functionally fitted as dependent on the X-ray luminosity and redshift, $P(R_X|L_X, z)$. It roughly spans over 6 decades ($-7 < R_X < -1$), and does not show any sign of bi-modality. It resulted that the probability of finding large values of the R_X ratio increases with decreasing X-ray luminosities and (possibly) with increasing redshift. No statistical significant difference was found between the radio properties of the X-ray absorbed ($N_H > 10^{22}$ cm⁻²) and unabsorbed AGN.

The measure of the probability distribution function of R_X allowed us to compute the kinetic luminosity function and the kinetic energy density which, at variance with what assumed in many galaxy evolution models, is observed to decrease of about a factor of five at redshift below 0.5. About half of the kinetic energy density results to be produced by the more radio quiet ($R_X < -4$) AGN.

In agreement with previous estimates, the AGN efficiency ϵ_{kin} in converting the accreted mass energy into kinetic power ($L_K = \epsilon_{kin} \dot{m} c^2$) is, on average, $\epsilon_{kin} \simeq 5 \times 10^{-3}$. The data suggest a possible increase of ϵ_{kin} at low redshifts.

Subject headings: galaxies: active – galaxies: evolution – galaxies: luminosity function, mass function – quasars: general – radio continuum: galaxies – X-rays: galaxies

1. INTRODUCTION

One of the main questions in galaxy formation evolution studies is the role of AGN feedback. According to popular AGN/galaxy co-evolutionary scenarios, once central super massive black holes (SMBHs) reaches masses $> 10^7 - 10^8 M_\odot$, the AGN can heat efficiently the galaxy interstellar matter (ISM) through winds, shocks, and high-energy radiation (Silk & Rees 1998, Fabian 1999), inhibiting further accretion and star-formation and making the galaxy colors redder (see e.g. Cattaneo et al. 2009 for a review).

Unfortunately there are still relatively few direct observations of AGN feedback, and its inclusion in galaxy evolution models is often performed using adjustable parameters to obtain the observed galaxy colors. Indeed, the results of the hydrodynamic N-body simulations (see, e.g. Di Matteo, Springel & Hernquist 2005; Springel 2005; Hopkins et al. 2005, 2006) and of the semi-analytical models of galaxy formation and evolution (SAMs, Monaco, Salucci & Danese 2000; Kauffmann & Haehnelt 2000; Volonteri, Haardt & Madau 2003; Granato et al. 2004; Menci et al. 2006, 2008; Croton et al. 2006; Bower et al. 2006; Marulli et al. 2008) depend on the AGN triggering mechanism and on the AGN feedback description. Is the feedback at work mainly during luminous AGN phases (the so called “quasar” or “radiative” mode, see e.g. Menci et al. 2008)? Or rather AGN

feedback proceeds continuously during the Cosmic time at a low rate (the so called “radio” or “kinetic” mode, see e.g. Croton et al. 2006, Marulli et al. 2008)?

In the first case the AGN feedback is associated to the the main radiative, and then X-ray, activity of the AGN which is thought to occur during episodes of accretion of cold gas coming from the galaxy ISM following galaxy encounters (e.g. Barnes & Hernquist 1992, Cavaliere & Vittorini 2000, Menci et al. 2008). In this scenario the AGN feedback is usually associated to the radiation and its total efficiency must be proportional to the AGN fraction (the AGN luminosity function vs. the galaxy luminosity function) and to the efficiency in releasing the AGN power in the galaxy ISM.

In the second case the radio feedback is assumed to be related to a low, uninterrupted and constant matter accretion rate onto the central SMBH ($\sim 10^{-5} M_\odot/\text{yr}$), coming from a quiescent inflow of gas cooling from the halo’s hot atmosphere (e.g. Monaco, Salucci & Danese 2000; Croton et al. 2006; Bower et al. 2006). This accretion rate is too small to contribute significantly to the bolometric output of the AGN. At variance, the mechanical effects of accelerated particles (jets), which are observed to be responsible for the large cavities on the intra-cluster medium revealed in the X-rays (e.g. McNamara et al. 2000), are believed to significantly perturb the ISM into radio galaxies (Saxton et al. 2005, Suther-

land & Bicknell 2007, Tortora et al. 2009; Krause & Gaibler 2009 and references therein). In this scenario, radio mode feedback total efficiency is thought to be proportional to the total accreted mass and then to the SMBH mass function and to the way the energy is channelled by the SMBH into its host galaxy and it is released in the ISM and intergalactic medium (IGM).

In the Croton et al. (2006) and Marulli et al. (2008) models, the radio-mode feedback is more effective in suppressing the cooling flows in the massive galaxies at late times (low redshifts). In the Cattaneo et al. (2006) model the cooling and star-formation are efficiently suppressed by the AGN radio feedback for haloes above a critical mass of $\sim 10^{12} M_\odot$ below $z \sim 3$. Bower et al. (2006) assume that the AGN energy injection is determined by a self-regulating feedback loop that starts when the luminosity exceeds some fraction of the Eddington luminosity. Recently, Shabala & Alexander (2009) have presented a galaxy formation and evolution model where the radio feedback occurs when the AGN accretion rate falls below a certain value and enters the advection dominated accretion flow (ADAF) regime. In their model the radio (and then kinetic) power is assumed to scale linearly with the accretion rate.

To support the above studies several authors have compared the mechanical (kinetic) luminosity function (LF) of radio sources to the bolometric AGN LFs (e.g. Best et al. 2006; Merloni & Heinz 2008; Shankar et al. 2008; Kording, Jester & Fender 2008; Cattaneo & Best 2009; Smolčić et al. 2009). All these works are based on the convolution of some empirical relation between the AGN kinetic power and its radio luminosity (see e.g. Willott et al. 1999; Best et al. 2006; Merloni & Heinz 2007; Birzan et al. 2008) with the AGN radio LF. As a consequence, these works deal with the AGN as a population and do not allow the inclusion in the models of the kinetic power of each single source during its evolution.

In the Croton et al. (2006) and Bower et al. (2006) SAMs it is not implemented any direct relation between the radio activity (feedback) and the X-ray luminosity (main episodes of mass accretion). However, a strong correlation between the X-ray (L_X) and radio luminosity of AGN is observed (e.g. Brinkmann et al. 2000), and L_X is a good proxy of the SMBH accretion rate \dot{m} , via the knowledge of the X-ray bolometric correction K_X and the efficiency ϵ of conversion of mass accretion into radiation

$$L_X = \frac{L_{bol}}{K_X} = \frac{\epsilon \dot{m} c^2}{(1 - \epsilon) K_X}, \quad (1)$$

where L_{bol} is the bolometric luminosity and it is assumed $\epsilon \simeq 0.1$ (see e.g. Marconi et al. 2004; Vasudevan & Fabian 2009).

The aim of this paper is therefore to estimate the AGN kinetic power linking the AGN radio emission to the accretion rate related to the AGN activity (the luminous phase). Our approach is then different from most of the above described models, and it can be considered, in some sort, as a quasar mode feedback (i.e. related to the luminous-accreting phases), but associated to the emitted radio-kinetic power. This can provide a robust quantitative root to a different kind of radio feedback, thus guiding its self-consistent inclusion in SAMs. In this framework, a very useful ingredient is the measure of

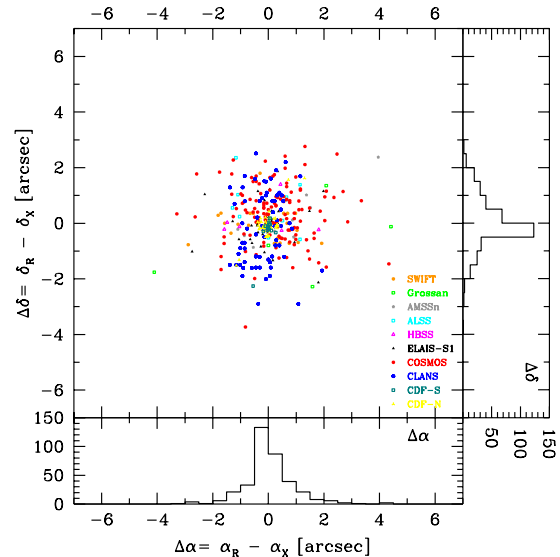


FIG. 1.— Distribution of the off-sets between the cross-correlated radio and X-ray sources.

the probability distribution function $P(R_X)$ of the ratio, R_X , between the AGN radio and hard X-ray luminosity [$R_X = \nu L_\nu(1.4 \text{ GHz})/L_X(2-10 \text{ keV})$]. To this purpose we used a data-set of more than 1600 X-ray selected AGN, observed in the radio band at 1.4 GHz, to measure $P(R_X)$ as a function of both luminosity and redshift: $P(R_X | L_X, z)$.

To estimate the AGN kinetic LF and its evolution, we first computed the radio LF by convolving $P(R_X | L_X, z)$, with the AGN 2-10 keV LF. We then convolved this radio LF with some of the relations (available from the literature) between the AGN radio and kinetic luminosities. As sanity tests, we first compared our results with previous studies on the relationship between the AGN X-ray and radio luminosities, and then we checked if previous measures of the radio LF and counts were correctly reproduced.

We adopted a flat cosmology with $H_0 = 70 \text{ km s}^{-1} \text{ Mpc}^{-1}$, $\Omega_M = 0.30$ and $\Omega_\Lambda = 0.70$. Unless otherwise stated, uncertainties are quoted at the 68% (1σ) confidence level.

2. THE DATA

As our objective was to use the R_X distribution in order to estimate the kinetic (radio) luminosity of the X-ray selected AGN, we had to measure a radio emission which was as much as possible causally linked (contemporary) with the observed X-ray activity (accretion). We then decided to measure the radio fluxes in a region as much close as possible to the AGN, therefore minimizing the contribution of objects like the radio lobes in FR II sources (Fanaroff & Riley 1974). For this reason we built up a large data-set of X-ray selected AGN (where redshift and N_H column densities estimates were available) observed at 1.4 GHz with a $\sim 1''$ typical spatial resolution (in our cosmology $1''$ corresponds, at maximum, to about 8 Kpc at $z \sim 2$). The cross correlation of the X-ray and radio catalogues was carried out inside a region with $5''$ of radius (almost less than or equal to the size of the central part of a galaxy like ours), following a maximum likelihood algorithm as described by Sutherland and Saunders (1992) and Ciliegi et al. (2003). In Fig-

ure 1 we show the off-sets between the X-ray and radio positions of the whole sample. These resulted to have a root mean square (rms) of $1.4''$. Therefore we expect to have (properly) preferentially included compact FRI radio sources in our cross-correlation and have excluded most of the contribution of the (especially bright) extended FRII radio lobes from our analysis (see sect 3.4.2 for a discussion on the contribution of the excluded FRII sources to the radio counts).

The total AGN sample was built up from a compilation of complete (i.e. with almost all redshift and N_H measures available) hard (mostly 2-10 keV) X-ray selected samples, with unabsorbed 2-10 keV luminosities higher than 10^{42} erg/s¹, as explained below.

2.1. The bright sample. The *SWIFT*, *INTEGRAL* and *HEAO-1* missions

In order to build up a large unbiased bright AGN (low redshift) sample, we joined the AGN samples recently generated from the *SWIFT* and *INTEGRAL* missions with the sample published by Grossan (1992) using the *HEAO-1* data. In the case of sources in common, priority was given first to the *SWIFT* data and then to the *INTEGRAL* ones and lastly to the sample of Grossan (1992).

The radio information was obtained via cross-correlation with the 1.4 GHz radio data taken from the FIRST VLA survey (Becker et al. 1995). The FIRST images have $1.8''$ large pixels, a typical rms sensitivity of 0.15 mJy and a resolution of $5''$. In the case of no radio detection a 5σ upper limit of 0.75 mJy was adopted. The large area NVSS (Condon et al. 1998) and SUMSS/ATCA (Mauch et al. 2003) radio surveys have positional uncertainties significantly larger than FIRST and therefore were not used in our analysis.

- *SWIFT*. The *SWIFT* sample we used is composed by 121 sources with high galactic latitude ($|b| > 15^\circ$) and detected with 14-195 keV fluxes brighter than 10^{-11} erg s⁻¹ cm⁻² (Tueller et al. 2008). All but one of the 121 sources have a redshift and an optical spectroscopic classification available (Tueller et al. 2008). 44 out of the 121 sources have been observed by *FIRST*. We limited our analysis to the 40 sources with 2-10 keV unabsorbed X-ray luminosity higher than 10^{42} erg/s: there are 18 broad optical emission line type 1 and 1.5 AGN (AGN1/1.5), 13 narrow emission line type 2 AGN (AGN2), 2 galaxies and 7 BL Lac in this sub-sample. In this and in all the other samples, all the BL Lac were excluded from our analysis as their radio fluxes are strongly amplified by the boosting of the relativistic radio jets. Therefore the AGN sample we used is composed by 33 sources in total (28 detected by FIRST). N_H column densities measures were provided by Tueller et al. (2008).
- *INTEGRAL*. We tried to complement the *SWIFT* data with the catalogue of 46 sources detected by

INTEGRAL at a 5σ significance level by Beckmann et al. (2006). However, after removing two sources without N_H measurements (from Sazonov et al. 2007), and 21 sources already included in the *SWIFT* sample, we ended with 18 sources which were not covered by the *FIRST* radio observations. Therefore, no source from the *INTEGRAL* catalogue from Beckmann et al. (2006) was included in our analysis.

- *GROSSAN*. The bright sample was eventually complemented with the sample of the *HEAO-1* sources described by Grossan (1992) as revised by Brusadin (2003). Brusadin et al. (2003) investigated, from the total sample of Grossan (1992), those 74 sources with 2-10 keV fluxes brighter than 2×10^{-11} erg s⁻¹ cm⁻². For 52 of these 74 sources the original optical counterparts were observed in the hard X-rays by at least one among the *ASCA*, *BeppoSAX* and *XMM-Newton* satellites. All the counterparts resulted to be real hard X-ray sources and a new estimate of the N_H column densities were derived. We used in this work a sub-sample of 66 objects, from the sample of Brusadin (2003), for which reliable measure of the N_H column densities were available.

Forty-one out of these 66 sources are not included in the *SWIFT* sample, and ten (10 AGN1/1.5) of them were observed by FIRST and have 2-10 keV X-ray unabsorbed luminosities higher than 10^{42} erg/s. Nine out of these last ten sources were also detected in the radio band by FIRST.

In summary, the bright sample contains 43 X-ray sources (28 AGN1, 13 AGN2, 2 galaxies; once the BL Lac were excluded) observed in the 1.4 GHz radio band by FIRST, with 37 detections.

2.2. AMSS

We selected those 87 sources of the *ASCA* Medium Sensitivity Survey (AMSS; as in Akiyama et al. 2003) having a S/N > 5.5 significant detection in the X-rays, $|b| > 30^\circ$ and $\delta > -20^\circ$; 76 of these sources were identified as AGN: seven clusters, 3 BL Lac and one star were excluded. Forty-three of these AGN were observed by FIRST (33 AGN1, 10 AGN2), and 11 were detected.

2.3. HBSS

We used the 67 sources of the *XMM-Newton* Hard Bright Sensitivity Survey (HBSS; Della Ceca et al. 2004) with 4.5-7.5 keV fluxes brighter than 7×10^{-14} erg s⁻¹ cm⁻² (which corresponds to a 2-10 keV limit of 3.5×10^{-13} erg s⁻¹ cm⁻² if a spectral index $\alpha = 0.7$, where $F_\nu \propto \nu^{-\alpha}$, is assumed). A subsample of 62 sources were used in our analysis after the exclusion of 2 stars, one cluster and 2 sources without a spectroscopic identification. Thirty-two sources were observed by FIRST (23 AGN1, 9 AGN2), while 6 were detected.

2.4. ALSS

The *ASCA* Large Sky Survey (ALSS) is a contiguous 7 deg² strip in the North Galactic Pole region (Ueda et al. 1999); we selected a sample with a limiting 2-10 keV flux

¹ Throughout this work we assumed that all the X-ray sources having 2-10 keV unabsorbed luminosities higher than 10^{42} erg/s are AGN (see e.g. Ranalli et al. 2003 for a study of the typical X-ray luminosities of star forming galaxies).

TABLE 1
THE SAMPLES

Sample	$N_{1.4}$	N_X	$\frac{N_{1.4}}{N_X}$	$F_{1.4}$	F_X	$\frac{F_{1.4}}{F_X}$
	(1)	(2)	(3)	(4)	(5)	(6)
Bright	37	43	0.86	750	2×10^{-11}	-6.3
AMSS	11	43	0.26	750	3×10^{-13}	-4.5
ALSS	9	30	0.30	750	1×10^{-13}	-4.0
HBSS	6	32	0.19	750	3.5×10^{-13}	-4.5
COSMOS	141	677	0.21	75	3×10^{-15}	-3.5
CLANS	69	139	0.50	19	3×10^{-15}	-4.1
ELAIS-S1	45	421	0.11	150	2×10^{-15}	-3.0
CDF-S	12	94	0.13	70	2.6×10^{-16}	-2.4
CDF-N	45	162	0.28	45	1.4×10^{-16}	-2.3
Total	375	1641	0.23

Notes. 1) Number of AGN detected at 1.4 GHz; 2) Number of X-ray AGN observed at 1.4 GHz; 3) Fraction of AGN detected at 1.4 GHz; 4) 1.4 GHz radio flux limit in μJy units; 5) 2-10 keV flux limit in $\text{erg s}^{-1} \text{cm}^{-2}$ units; 6) $\log[\nu F_\nu(1.4 \text{ GHz})/F_\nu(2-10 \text{ keV})]$.

of $1 \times 10^{-13} \text{ erg s}^{-1} \text{cm}^{-2}$ from Akiyama et al. (2000). This sample contains 30 AGN (25 AGN1, 5 AGN2), as well as two clusters, one star and one object without spectroscopic identification, which were excluded from our analysis. All the 30 AGN were observed by FIRST, while nine were detected.

2.5. COSMOS

In order to use the COSMOS survey, we used the XMM-Newton X-ray catalogue by Cappelluti et al. (2009) with a limiting 2-10 keV flux of $\sim 3 \times 10^{-15} \text{ erg s}^{-1} \text{cm}^{-2}$ and cross-correlated with the spectroscopic identifications by Trump et al. (2009) and the photometric redshift estimates from Ilbert et al. (2009) and Salvato et al. (2009). The N_H measures were derived by our analysis of the hardness ratios (HR). The radio data were obtained from Schinnerer et al. (2007). In order to allow a uniform radio coverage (with 1.4 GHz rms of $15 \mu\text{Jy}$) the central 1 deg^2 squared area with limits $9^h58^m40^s < \alpha < 10^h2^m40^s$ and $1^\circ42' < \delta < 2^\circ42'$ was used. In this area the X-ray catalogue contains 712 sources. 677 are extragalactic with a redshift measure available and 2-10 keV luminosity higher than 10^{42} erg/s . 389 have a spectroscopic redshift (186 AGN1, 52 AGN2, 71 emission line galaxies, ELG, 32 normal passive galaxies, GAL, 48 no class), while 288 have only a photometric redshift estimate available. We used all the radio detections with 1.4 GHz flux limits brighter than $75 \mu\text{Jy}$ (5σ) and used the same threshold as an upper limit for all the remaining sources even though lower flux detections were available in some cases. In total 141 out of the 677 sources, contained in our selected region of the COSMOS field, were detected in the 1.4 GHz radio band.

2.6. ELAIS-S1

In the European Large Area *ISO* Survey field S1 (ELAIS-S1) we used the catalogue of the XMM-Newton sources published by Puccetti et al. (2006), which reaches a 2-10 keV flux limit of $2 \times 10^{-15} \text{ erg s}^{-1} \text{cm}^{-2}$. The spectroscopic identifications and classifications provided by Feruglio et al. (2008) and Sacchi et al. (2009) were used, while the 1.4 GHz radio data (with a 5σ limit of $150 \mu\text{Jy}$) were taken from Middelberg et al. (2009).

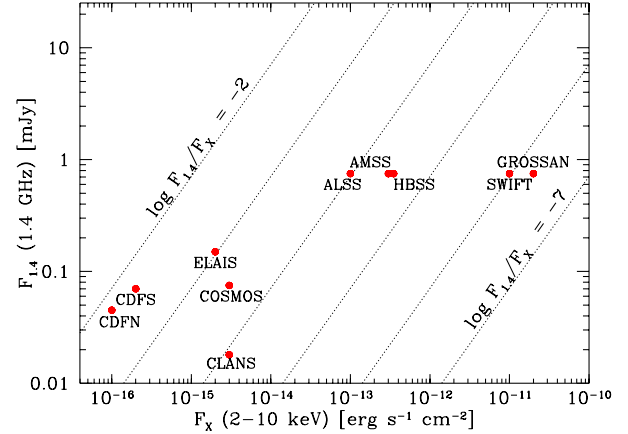


FIG. 2.— Lower (5σ) radio flux 1.4 GHz limits as a function of the lower X-ray 2-10 keV flux limits of the samples. Dashed lines show the loci with equal $\nu F_\nu(1.4 \text{ GHz})/F_\nu(2-10 \text{ keV})$ ratio as shown by the labels.

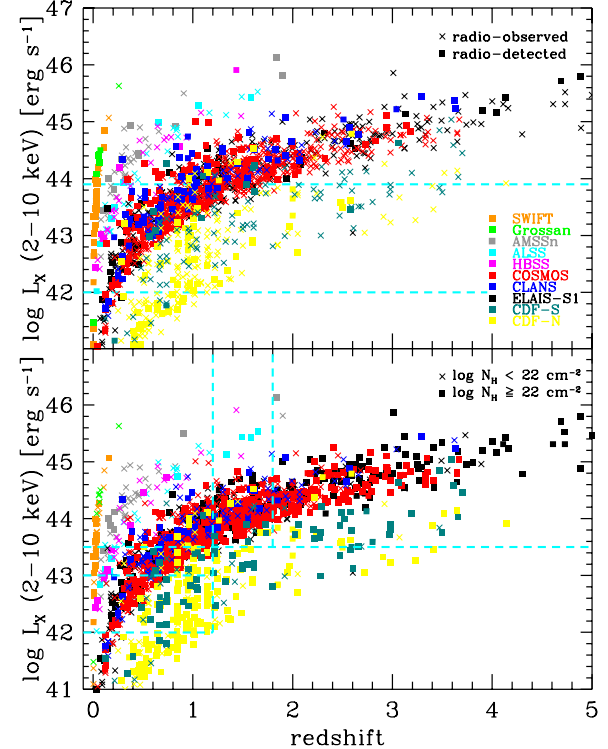


FIG. 3.— 2-10 keV X-ray de-absorbed luminosity as a function of the redshift for all the AGN observed at 1.4 GHz used in this work. *Top.* Crosses indicate the sources observed in the radio band, while filled squares show those objects which have been detected in the radio. The dashed lines show the two z - L_X regions used to measure the distribution of R_X at $R_X < -4$. *Bottom.* Crosses indicate the sources with $\log N_H < 22 \text{ cm}^{-2}$, while filled squares show those AGN with $\log N_H \geq 22 \text{ cm}^{-2}$. The dashed lines show the five z - L_X regions used to measure the distribution of R_X at $R_X \geq -4$.

The whole sample contains 421 extragalactic sources with a redshift measure available and 2-10 keV luminosity higher than 10^{42} erg/s : 240 have been identified and classified spectroscopically (116 AGN1, 34 AGN2, 68 ELG, 22 GAL), while 181 have a photometric redshift available. Forty-five out of these 421 AGN were detected at 1.4 GHz above the $150 \mu\text{Jy}$ limit.

2.7. CLANS

In the Chandra Lockman Area North Survey (CLANS) field the X-ray data were taken from Trouille et al. (2008), which also publish the spectroscopic and photometric redshift measures. Our sample consists of the sources with $S/N > 3$ detections in the hard 2-8 keV band and includes in the circular area with radius of 0.32 deg and center in: $\alpha 10^h 46'$, $\delta 59^\circ 01'$ (J2000). This area contains 139 extragalactic sources with a redshift measure available and 2-10 keV luminosity higher than 10^{42} erg/s: 113 sources were spectroscopically identified (58 AGN1, 34 AGN2, 16 ELG, 5 galaxies), while 29 sources have a photometric redshift available. The N_H measures were derived from the analysis of the HR. Radio data were obtained from Owen et al. (2008). We conservatively modeled the spatial dependence of the (5σ) radio flux limits, which vary from $18.5 \mu\text{Jy}$ in the central region up to $59.2 \mu\text{Jy}$ near the edges. Sixty-nine out of the 139 sources were radio-detected.

2.8. CDFS

In the *Chandra* Deep Field South (CDFS) the subsample of the GOODS-S X-ray sources from the catalogue of Alexander et al. (2003) was used. The whole sample consists of the 94 point like extragalactic sources over a 2-10 keV flux limit (at the aim point) of 2.6×10^{-16} erg $\text{s}^{-1} \text{cm}^{-2}$ with a redshift measure available and a 2-10 keV luminosity higher than 10^{42} erg/s. Spectroscopic identifications for 69 sources, as well as 25 photometric redshifts, were obtained from (Brusa et al. 2009b). Twenty-nine sources were identified as AGN (17 AGN1, 12 AGN2), 39 as ELG and one as a galaxy. The radio data were taken from Miller et al. (2008) and have a 1.4 GHz 5σ flux limit of $70 \mu\text{Jy}$. Twelve sources were radio-detected.

2.9. CDFN

In the *Chandra* Deep Field North (CDFN) we used the 296 2-8 keV X-ray sources detected by *Chandra* within the GOODS-N area with a 2-10 keV flux limit (at the aim point) of 1.4×10^{-16} erg $\text{s}^{-1} \text{cm}^{-2}$ by Alexander et al. (2003). To convert the 2-8 keV fluxes in the 2-10 keV band a spectral index $\alpha=0.4$ were assumed. The spectroscopic identifications were taken from Trouille et al. (2008). The sample consists of 162 extragalactic sources with a redshift measure available and 2-10 keV luminosity higher than 10^{42} erg/s: 104 sources were spectroscopically identified (16 AGN1, 20 AGN2, 46 ELG, 22 galaxies), while 50 sources have a photometric redshift; eight other spectroscopical redshift were retrieved from literature. N_H values were obtained from the analysis of the HR. The radio information were obtained from the new data reduction from Biggs & Ivison (2006) of the 1.4 GHz VLA observation of Richards (2000). Forty-five out of the 162 extragalactic sources were identified in the 1.4 GHz band over a (5σ) flux limit of $45 \mu\text{Jy}$.

2.10. The whole X-ray sample

In summary, our radio observed hard X-ray selected extragalactic total sample contains 1641 sources with both redshifts (either spectroscopic or photometric) and N_H column densities measured, and with un-absorbed 2-10

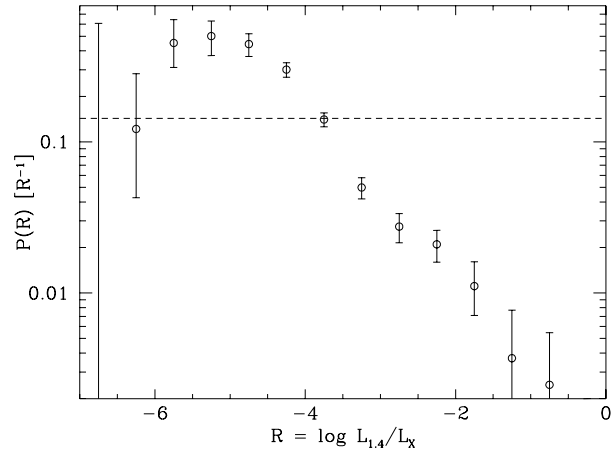


FIG. 4.— Probability distribution function of R_X for the full sample under the assumption of a flat distribution (dashed line).

keV luminosities higher than 10^{42} erg/s². 1003 sources have N_H higher than 10^{22}cm^{-2} (hereafter defined “X-ray absorbed”). 375 (23%) sources were detected in the 1.4 GHz radio band. See Table 1 for a summary of the main properties of all samples used. In Figure 2 we show the (5σ) radio 1.4 GHz flux limits of each survey as a function of their deepest 2-10 keV X-ray flux limits. The distribution of the de-absorbed X-ray luminosity of all sources (distinguished according to radio detection and X-ray absorption classes) as a function of redshift is shown in Figure 3.

3. THE DISTRIBUTION OF THE $R=L_R/L_X$ RATIO

3.1. The method

We searched for a functional fit of the probability distribution function of R_X , as a function of the X-ray luminosity, L_X , and the redshift: $P(R_X|L_X, z)$. The method is based on the comparison, through χ^2 estimators, of the observed and expected numbers of AGNs (in the L_X - z - R_X space) obtained by taking into account the observational selection effects (i.e. the radio flux limits) of each sample. Once a probability distribution function $P(R_X|L_X, z)$ is assumed, the number of expected AGNs in a given bin of the L_X - z - R_X space is the result of the sum, over the number of all AGN contained in the L_X - z bin, of the expected number of AGNs contained in that bin of R_X , by taking into account the radio flux limits on each source. This method reproduces the observations and consequently properly takes into account both the radio detections and the upper limits (see La Franca et al. 1994, 1997, 2002, 2005 for similar applications).

3.2. The fit

As a first test we assumed a constant (flat) probability distribution function of R_X in the range $-7 < R_X < 0$ (see Figure 4). This distribution, although different from the true one, allows to see which is the shape of the average true distribution via the analysis, in each bin, of the deviations of the observed numbers of AGN from the

² Other X-ray samples, such as HELLAS2XMM (Fiore et al. 2003; Cocchia et al. 2007), the XMM/Lockman Hole (Brunner et al. 2008) and the XMM Medium Survey (Barcons et al. 2007), were not included in our work because unbiased, homogeneous and dedicated radio 1.4 GHz observations were not available.

TABLE 2
BEST FIT PARAMETERS

Model	N	γ_R	γ_L	R_C	α_L	α_z	$\chi^2/\text{d.o.f.}$	$P(\chi^2)$
1 - box	670.17/12	0
2 - no dep	1.0620	0.476	1.93	-4.313	46.73/20	6.4×10^{-4}
3 - dep z	1.0899	0.467	1.69	-4.319	...	0.028	41.98/19	0.020
4 - dep L	1.0652	0.429	1.70	-4.386	0.056	...	30.19/19	0.049
5 - dep L,z	1.0230	0.369	1.69	-4.578	0.109	-0.066	22.77/18	0.200
1σ errors		+0.040 -0.031	+0.18 -0.31	+0.110 -0.086	+0.019 -0.025	+0.024 -0.016		

expected ones. Figure 4 shows that the average distribution function is a-symmetrical with a long tail at large R_X values.

We then divided the L_X - z - R_X space into 23 independent bins, which were chosen in order to look for possible dependences of the $P(R_X|L_X, z)$ shape on the luminosity and redshift (see Figure 3 for a representation of the L_X - z regions) while ensuring that about, at least, 10 AGN were observed in each bin (see Figure 5).

After several trials, we found that the probability distribution function of R_X is, indeed, a-symmetrical, showing a maximum at $R_X=R_0$, where the median is located. At R_X larger than R_0 the distribution is fairly well represented by a Lorentz function having width γ_r , which provides a shallow decline at large R_X values, while at R_X smaller than R_0 the exponent 2 of the Lorentz function is better substituted by an exponent 4 which gives a wider shoulder at $R_X \lesssim R_0$ and then a steep decline at even lower R_X . The width of the left ($R_X < R_0$) part of the distribution is controlled by the γ_l parameter. Therefore the probability distribution function $P(R_X|L_X, z)$ is expressed by the following formula:

$$P(R_X) = \begin{cases} \frac{N}{A\pi\gamma_l \left[1 + \left(\frac{R_0(L_X, z) - R_X}{\gamma_l}\right)^4\right]} & (R_X < R_0) \\ \frac{A N}{\pi\gamma_r \left[1 + \left(\frac{R_X - R_0(L_X, z)}{\gamma_r}\right)^2\right]} & (R_X \geq R_0), \end{cases} \quad (2)$$

where, in order to obtain a continuous function at $R_X=R_0$ results $A = \sqrt{\gamma_r/\gamma_l}$, and the parameter N is constrained by the probability normalization requirement: $\int P(R_X|L_X, z) dR_X = 1$. For $0.3 \leq z \leq 3.0$ and $42.2 \leq \text{Log} L_X \leq 47.0$, we allowed to vary, as a function of L_X and z , the position of the maximum (median) R_0 of the distribution, according to the following formula:

$$R_0 = R_C [\alpha_L (\text{Log} L_X - 44) + 1] [\alpha_z (z - 0.5) + 1]. \quad (3)$$

At redshifts and luminosities outside these ranges, R_0 was kept constant, equal to the values assumed at the limits of the ranges.

In Table 2 the results of the fits carried out using this parameterization are reported. Confidence regions of each parameter were obtained by computing χ^2 at a number of values around the best-fit solution, while leaving the other parameters free to float (see Lampton et al. 1976). The 68% confidence regions quoted correspond to $\Delta\chi^2=1$.

The solution without dependences on both the luminosity and the redshift is rejected by the χ^2 test, while

the solutions either depending only on luminosity or redshift provide barely acceptable fits to the data. A fairly good fit to the data (20% χ^2 probability) is instead provided by the solution #5 where both a dependence on the luminosity and the redshift is allowed. However, it should be noted that the parameter of the redshift dependence, α_z , is different from zero only at 3σ confidence level.

The data and the shape of the best fit #5 probability distribution function are shown in Figure 5, while the corresponding dependences of R_0 on L_X and z are shown in Figure 6. In Figure 7 we show the shape of the best fit #5 probability distribution function in different bins of X-ray luminosity and redshift, with evidence (the continuous lines) to the part which is actually constrained by the data.

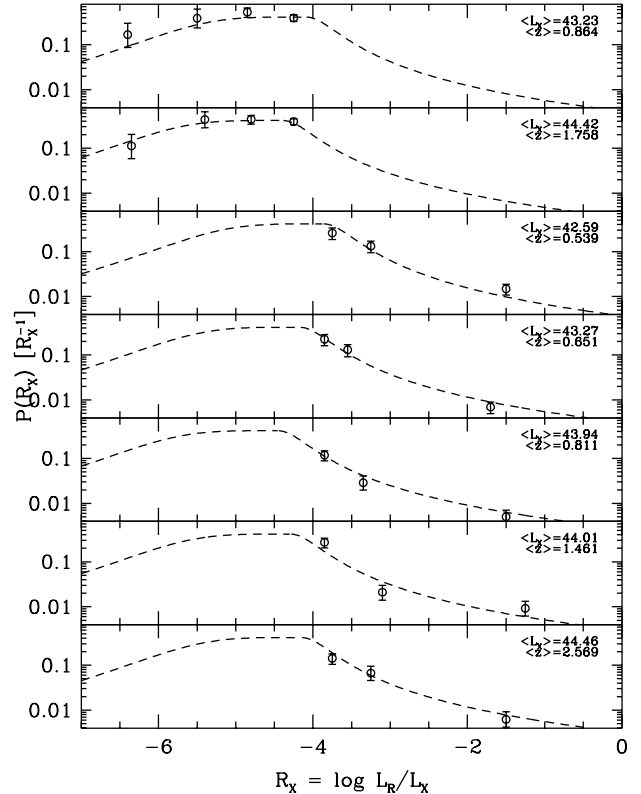


FIG. 5.— Probability distribution function of R_X as a function of L_X and z . The dashed line shows our best fit solution #5 (see Table 2). The limits in the L_X - z space of the seven regions used are shown in Figure 3.

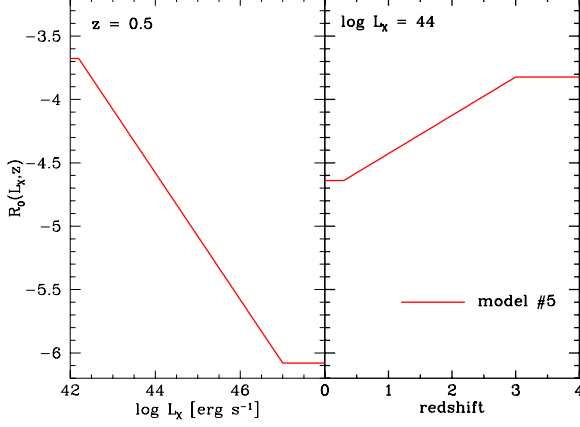


FIG. 6.— Dependence of the position of the median R_0 of the probability distribution function on L_X and z as computed in our best fit solution #5 (red continuous line; see text and Table 2).

3.3. Dependence on N_H

We did not find any significant dependence of the $P(R_X|L_X, z)$ distribution on the N_H column densities. The sample was divided into absorbed ($N_H > 10^{22} \text{ cm}^{-2}$) and un-absorbed AGN. For both sub-samples the χ^2 test on the best fit solution #5 (even with a different sampling in order to always observe at least 10 objects in each bin) provided probabilities larger than 10% (up to 70%), and was then not able to reject our best fit distribution. This result is in agreement with the analysis of the X-ray absorption properties of the faint radio sources

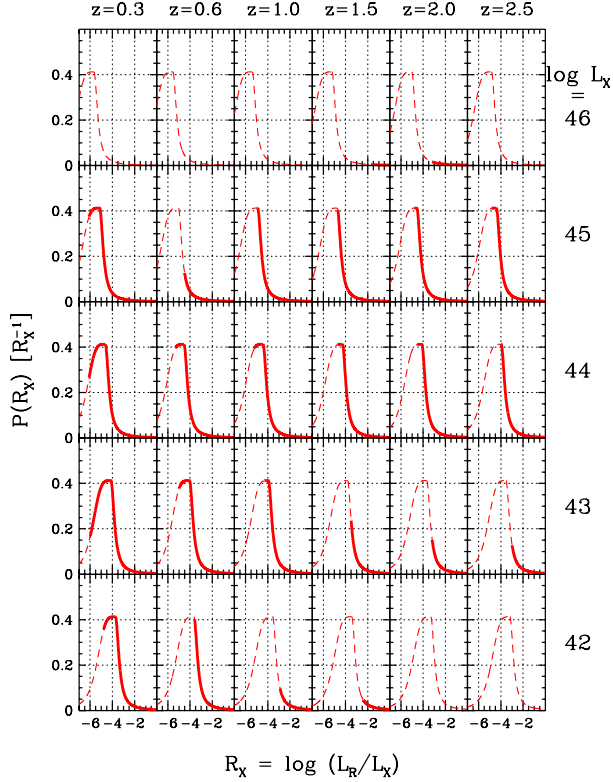


FIG. 7.— Probability distribution function in different bins of L_X and z , as computed in our best fit solution #5 (see Table 2). The continuous line shows the range of R_X where the fit is constrained by the data, while the dashed line shows where the distribution is extrapolated.

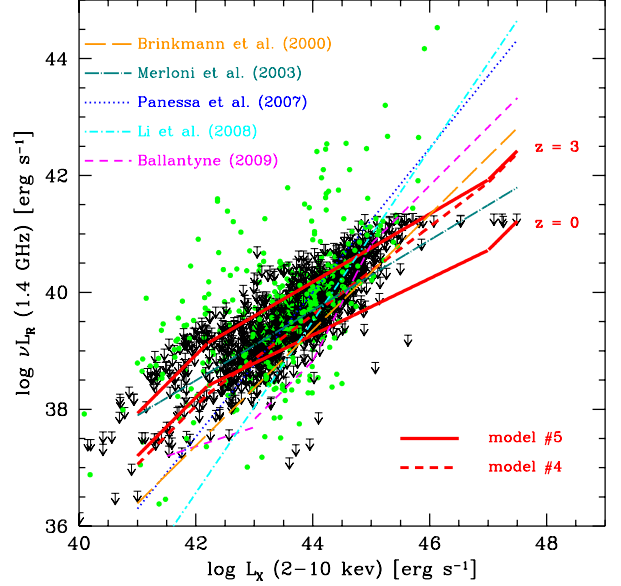


FIG. 8.— 1.4 GHz luminosity as a function of the intrinsic 2-10 keV luminosity of all AGN contained in our sample (only the AGN with $\log L_X \geq 42$ have been used in our analysis). Radio detection are shown by green dots, while radio upper limits are shown by arrows. The dependence, according to fit #5, of the position of the median R_0 of the $P(R_X|L_X, z)$ distribution (see eq. 3) at redshift 0 and 3 is shown by red continuous lines. For comparison the relations derived by Brinkmann et al. (2000; orange long dashed), Panessa et al. (2007; blue dotted), and Ballantyne (2009; magenta dashed) are shown. The relations derived by the measure of the AGN fundamental plane by Merloni et al. (2003) and Li et al. (2008) are shown (green dot-dashed and cyan dot-dashed lines, respectively) assuming a fixed BH mass of $10^8 M_\odot$ (see text).

of the CDFS by Tozzi et al. (2009).

3.4. Sanity checks

3.4.1. The L_R - L_X relation

We compared our measure of the probability distribution function of R_X with previous measures on the relationship between the AGN radio and X-ray luminosities. In Figure 8 we show the 1.4 GHz luminosity as a function of the intrinsic 2-10 keV luminosity for all the sources of our sample. Our analysis differs from many previous studies where single general log-log linear relations were derived. In these studies, even when the presence of censored data, or data with errors in both axes (see e.g. La Franca et al. 1995), were taken into account, it was assumed the presence of a symmetrical (usually Gaussian) distribution of the deviations from the best fit relation, which were attributed to an intrinsic scatter. Our method, instead, by taking into account all the censored data, allows to measure the *shape* of the distribution of the intrinsic scatter and its possible dependences on other variables (such as the luminosity and redshift in our case). In Figure 8 we compare our best fit solution #5 with the relations derived by other authors such as Brinkmann et al. (2000) in the soft 0.5-2 keV band³, Merloni et al. (2003), Panessa et al. (2007), Li et al. (2008) and Ballantyne (2009; for the radio quiet AGN) in the 2-10 keV band. The relations by Merloni et

³ An X-ray spectral index $\alpha=0.7$ was assumed to convert the 0.5-2 keV luminosities into 2-10 keV luminosities.

al. (2003) and Li et al. (2008) were derived from their measure of the AGN fundamental plane (i.e. including also a dependence on the BH mass), assuming a fixed BH mass of $10^8 M_\odot$.

As our measured distribution function is a-symmetrical and depends on the redshift, the comparison is not straightforward (in Figure 8 we plot the position of the median R_0 of the distribution at redshifts 0 and 3). It results that our best fit solution #5 of the dependence of the 1.4 GHz luminosity on the 2-10 keV luminosity is flatter than obtained in previous works. Our fitted relation corresponds to a power-law $L_R \propto L_X^\alpha$ with indexes $\alpha=0.48$ and $\alpha=0.58$ at redshifts 0 and 3, respectively. The relations fitted by the other authors have instead a wide range of power-law indexes ($0.6 \lesssim \alpha \lesssim 1.5$), systematically steeper than our result. This difference is partly caused by our new method used to measure the L_R - L_X relation but it is also caused by our introduction (and measure) of a dependence on the redshift of the average R_X values. In fact, as shown in Figure 8, our solution #4, obtained without the inclusion of a redshift dependence, results in a steeper slope, having a power-law index $\alpha = 0.75$. Figure 8 also shows that the fundamental plane by Merloni et al. (2003) has a power-law index ($\alpha=0.60$) close to our best fit estimate ($\alpha=0.48$ - 0.58), and for BH masses of $10^8 M_\odot$ is located between our best fit relations at redshift 0 and 3. In the fundamental plane estimate by Merloni et al. (2003) R_X has also a dependence on the BH mass of the type $\propto 0.78 \log(M_{\text{BH}})$. This implies that our estimates at redshift 0 and 3 are roughly similar to the fundamental plane measures for BH masses of 10^7 and $10^9 M_\odot$, respectively. Therefore, as in our (and all flux limited) samples, high redshift AGN are on average more luminous, and thus probably host on average more massive BH, we can infer that our measure of the increase with the redshift of the median of the R_X distribution is qualitatively in agreement with the AGN fundamental plane measures where an increase of the average R_X with the BH masses is observed.

3.4.2. The 1.4 GHz luminosity function and counts

We then verified if the measured probability distribution function of R_X , once convolved with the 2-10 keV LF, properly reproduces (taking into account the uncertainties) independent previous measures of the 1.4 GHz LF, $\Phi_R(L_{1.4}, z)$, and integral counts, $N(> S)$. We used the 2-10 keV LF, $\Phi_X(L_X, z)$, as measured by La Franca et al. (2005), and modified by allowing a steep exponential decline of the AGN density at redshifts larger than $z = 2.7$, as measured by Brusa et al. (2009a). As discussed in La Franca et al. (2005), the density of Compton thick AGN with $24 < \log N_H \leq 26 \text{ cm}^{-2}$ was assumed to be equal to the density of the Compton thin AGN with $22 < \log N_H \leq 24 \text{ cm}^{-2}$ (this assumption resulted to properly reproduce the cosmic X-ray background). The X-ray LF can be converted into a radio LF by the formula:

$$\Phi_R(L_{1.4}, z) = \int P(R_X | L_X, z) \Phi_X(L_X, z) d \log L_X. \quad (4)$$

The X-ray LF was integrated starting from an X-ray luminosity $\log L_X = 41 \text{ erg/s}$. The predicted radio LF is shown in Figure 9 and compared with the 1.4 GHz radio LF measured by Smolčić et al. (2009). As discussed in Smolčić et al. (2009), this radio LF includes (like in

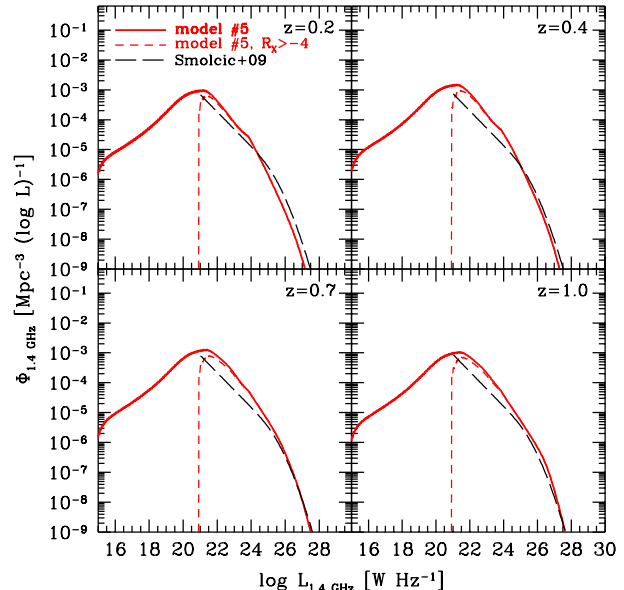


FIG. 9.— Predicted 1.4 GHz radio LF according to our fit #5, at redshifts 0.2, 0.4, 0.7 and 1.0 (red continuous lines). The dashed red lines show the part of the LF reproduced by the $P(R_X)$ distribution with $R_X > -4$. The black long dashed lines show the radio luminosity function as estimated by Smolčić et al. (2009).

our measure of the distribution of R_X) mostly the FRI sources. Although also affected by the uncertainties on the measure of the X-ray LF by La Franca et al. (2005), our best fit #5 of the probability distribution function of R_X provides a fairly good reproduction of the FRI radio luminosity function.

As a result of this computation, our estimate of the distribution of R_X allows to predict the AGN FRI radio LF at luminosities smaller than $L_{1.4} = 10^{21} \text{ W Hz}^{-1}$, never probed before. However at these low radio luminosities the AGN could be overwhelmed by the radio emission of the hosting galaxy because during periods of strong star formation activity the supernovae remnants accelerate cosmic rays which radiate synchrotron emission in local magnetic fields. According to Ranalli et al. (2003), strong star forming galaxies ($\sim 10^2 M_\odot/\text{yr}$) have about 10^{42} erg/s 2-10 keV luminosities, and, in general, in all star forming galaxies a linear relation between the 1.4 GHz radio and the 2-10 keV luminosities is observed, which corresponds to a value $R_X \simeq -2.0$. At face value this would imply that for the lowest luminosity AGN ($\log L_X \simeq 42$ - 43 erg/s) most of our measure of the $P(R_X)$ distribution (which spans in the range $-7 < R_X < -1$) could be contaminated if the hosting galaxies are undergoing a strong star formation activity. However, as shown in Figure 7, at low R_X values the $P(R_X)$ distribution is mostly measured from AGN with $43 < \log L_X < 45 \text{ erg/s}$, and redshift lower than $z \sim 0.5$. At these low redshifts it is very unlikely for galaxies to harbor a star formation stronger than $\sim 10 M_\odot/\text{yr}$ (Elbaz et al. 2007; Noeske et al. 2007), which roughly corresponds to an emission in the 2-10 keV band of $\log L_X \sim 41 \text{ erg/s}$ (Ranalli et al. 2003). Therefore, for example, in a low redshift AGN with $\log L_X \sim 44 \text{ erg/s}$, having an hosting galaxy whose star formation emits a 2-10 keV luminosity of $\log L_X \sim 41 \text{ erg/s}$, the corresponding radio emission (having an intrinsic $R_X \simeq -2.0$) can contaminate our mea-

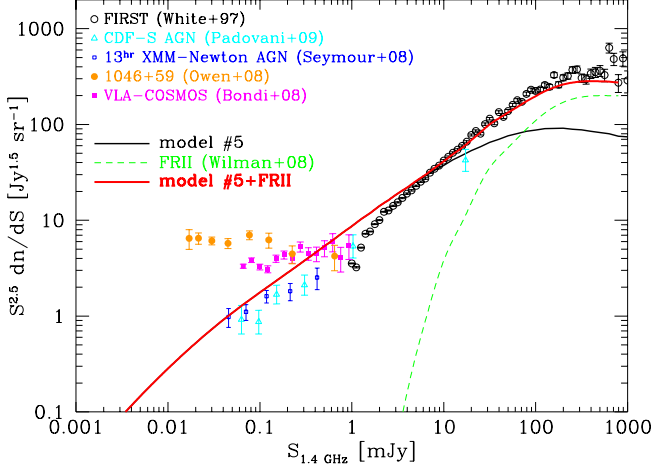


FIG. 10.— Euclidean differential radio counts at 1.4 GHz. The black continuous line shows the expected counts according to the convolution of the $P(R_X)$ distribution of fit # 5 (see Table 2) with the X-ray LF of La Franca et al. (2005). The green dashed line shows the radio counts produced by the FR II sources according to Wilman et al. (2008). The red continuous line is the sum of our predicted counts (the black line) with the counts of the FR II sources (green dashed line). Radio counts measures are shown by black open circles (FIRST; White et al. 1997), magenta filled squares (Bondi et al. 2008) and orange filled circles (Owen et al. 2008). Blue open squares and cyan open triangles show the AGN counts estimated by Seymour et al. (2008) and Padovani et al. (2009), respectively.

sure of the R_X distribution only for R_X values smaller than -5 . We can then conclude that only at the lowest R_X values ($\lesssim -5$) our measure of the $P(R_X)$ distribution is potentially affected by a contamination from the radio emission due to the star formation activity of the AGN hosting galaxies.

We used the above computed radio LF (eq. 4) to derive the expected integral counts $N(>S)$ from the following equation:

$$N(>S) = \frac{1}{4\pi} \int \frac{dv}{dz} dz \int_{S k(z) 4\pi d_l^2(z)}^{L_{max}} \Phi(L_{1.4}, z) d\log L_{1.4}, \quad (5)$$

where $k(z) = (1+z)^{\alpha_R-1}$ (with $F_\nu \propto \nu^{-\alpha_R}$ and $\alpha_R = 0.5$) is the radio k -correction, $d_l(z)$ the luminosity distance, and the integral counts are measured in sr^{-1} units. The predicted radio counts are shown in Figure 10. As our measured distribution of R_X represents only the FRI population (see discussion in sect. 2), in order to reproduce the total radio counts, the contribution derived from the LF of the FR II population (as measured by Wilman et al. 2008) was added. The reproduced counts are in good agreement with the observations. At 1.4 GHz fluxes below 1 mJy the euclidean radio counts flatten, due to the appearance of the population of the star forming galaxies. In this context, it is matter of discussion which is the fraction of the AGN at these fluxes. Our results agree with recent estimates of the AGN contributions to the sub-millijansky radio counts from Seymour et al. (2008) and Padovani et al. (2009). Similar results (at these fluxes) have also been obtained from semi-empirical simulations of the extragalactic radio counts by Jarvis & Rawlings (2004), Wilman et al. (2008) and Ballantyne (2009).

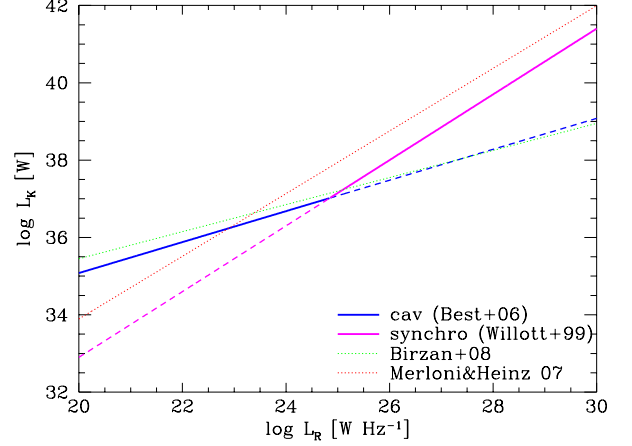


FIG. 11.— Kinetic luminosity as function of the radio luminosity as estimated by Willott et al. (1999; magenta lines), Best et al. (2006; blue lines), Merloni & Heinz (2007; red dotted line) and Birzan et al. (2008; green dotted line). In our work we used the combination of the relations from Best et al. (2006) and Willott et al. (1999) at low and high luminosities, respectively (the two continuous lines).

4. THE KINETIC LUMINOSITY FUNCTION

Once the radio LF of the FRI sources is measured (Equation 4 and Figure 9), in order to derive the kinetic mechanical LF and its evolution, we should convolve the 1.4 GHz LF with a relation which converts the radio luminosity $L_{1.4}$ into a mechanical power L_K . In the last decade, several authors have worked on the estimate of this relation (Willott et al. 1999; Birzan et al. 2004, 2008; Best et al. 2006; Heinz et al. 2007; Merloni & Heinz 2008). Following the discussion of Cattaneo and Best (2009) we used two different estimates which are representative of two different luminosity regimes. At high radio luminosities ($L_{1.4} \gtrsim 10^{25} \text{ W Hz}^{-1}$), Willott et al. (1999) used the minimum entropy density that the plasma radio lobes must have in order to emit the observed synchrotron radiation and obtained (see Figure 11):

$$L_K = 1.4 \times 10^{37} \left(\frac{L_{1.4 \text{ GHz}}}{10^{25} \text{ W Hz}^{-1}} \right)^{0.85} \text{ W}. \quad (6)$$

A second approach is to infer L_K from the mechanical work that the lobes do on the surrounding hot gas. The expanding lobes of relativistic synchrotron-emitting plasma open cavities (of volume V) in the ambient thermal X-ray emitting plasma. The minimum work in inflating these cavities is done for reversible (quasi-static) inflation and equals pV , where p is the pressure of the ambient gas. Best et al. (2006) derived a relation between radio and mechanical luminosity based upon this estimate for the energy associated with these cavities, combined with an estimate of the cavity ages from the buoyancy timescale (from Birzan et al. 2004). Comparing the mechanical luminosities of 19 nearby radio sources that have associated X-ray cavities with their 1.4 GHz monochromatic radio luminosities leads to a relation

$$L_K = 1.2 \times 10^{37} \left(\frac{L_{1.4 \text{ GHz}}}{10^{25} \text{ W Hz}^{-1}} \right)^{0.40} \text{ W}, \quad (7)$$

which is better suited for low luminosities ($L_{1.4} \lesssim 10^{25} \text{ W Hz}^{-1}$) and is close to the estimate by Birzan et al.

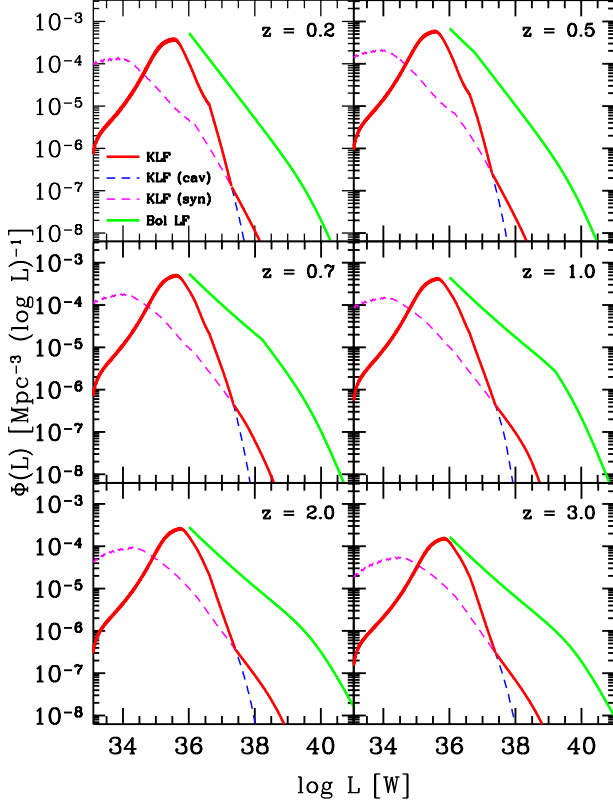


FIG. 12.— Bolometric radiative (green continuous line) and kinetic AGN LF. The magenta and blue lines show the kinetic LF predicted using the relations linking the radio and kinetic luminosities of Willott et al. (1999) and Best et al. (2006) respectively. The red line is the result obtained using the combination of the relations of Willott et al. (1999) and Best et al. (2006) at high and low luminosities respectively (see text and Figure 11).

(2008; see Figure 11). Using a similar method, Merloni & Heinz (2008) obtained at high radio luminosities, a relation similar to the one by Willott et al. (1999) but with about 0.5-1 dex higher kinetic luminosities (see Figure 11).

In this work (as in Cattaneo and Best 2009) we used Equation 6 at high luminosities ($L_{1.4} \gtrsim 10^{25}$ W Hz $^{-1}$) and Equation 7 at lower luminosities. Using these relations, once derived the radio LF from the X-ray LF and the R_X distribution according to Equation 4, we can estimate the kinetic LF, $\Phi_K(L_K, z)$, by the formula

$$\Phi_K(L_K, z) = \frac{dN(L_K, z)}{dV d\log L_K} = \Phi_{1.4}(L_{1.4}(L_K), z) \frac{d\log L_{1.4}}{d\log L_K}, \quad (8)$$

while the bolometric radiative LF, $\Phi_{rad}(L_B, z)$, is derived from the X-ray LF, via the bolometric correction $L_B = K_X(L_X)L_X$, by

$$\Phi_{rad}(L_B, z) = \frac{dN(L_B, z)}{dV d\log L_B} = \Phi_X(L_X(L_B), z) \frac{d\log L_X}{d\log L_B}, \quad (9)$$

where for $K_X(L_X)$ we used the relation from Marconi et al. (2004). Both the, so derived, kinetic and radiative (bolometric) LF are shown in Figure 12, while in Figure 13 the kinetic power density, $L_K \Phi_K(L_K, z)$, as function of the kinetic luminosity is shown.

By integrating in luminosity the above derived kinetic

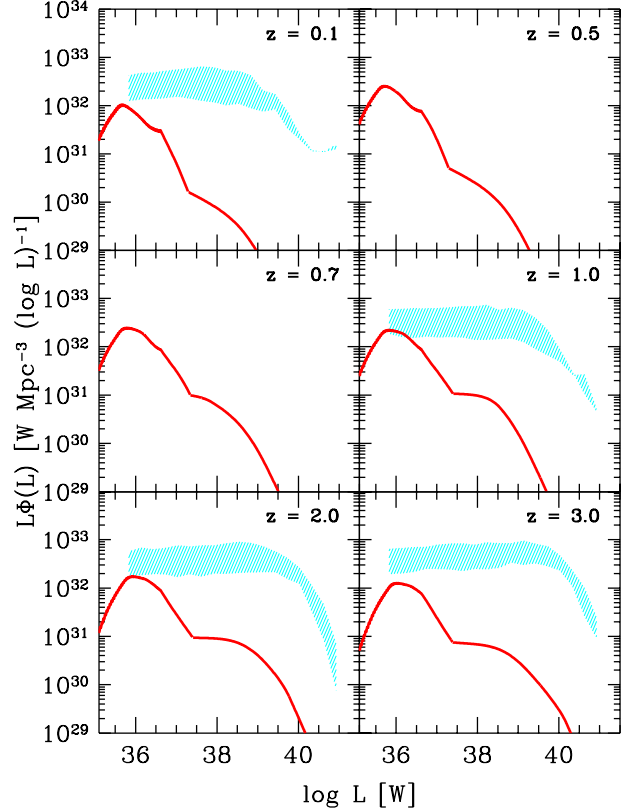


FIG. 13.— Kinetic power density, $L_K \Phi_K(L_K, z)$, as function of the kinetic luminosity according to the fit solution #5 (red continuous line). The results by Merloni & Heinz (2008) are shown by a cyan shaded area.

and radiative (bolometric) LF it is possible to estimate the dependence of the AGN mechanical and radiative power per unit cosmic volume as a function of redshift,

$$\Omega_K(z) = \int L_K(L_{1.4}) \Phi_{1.4}(L_{1.4}, z) d\log L_{1.4}, \quad (10)$$

and

$$\Omega_{rad}(z) = \int L_{bol}(L_X) \Phi_X(L_X, z) d\log L_X, \quad (11)$$

which are shown in Figure 14. As both the above equations depends on the X-ray luminosity function (see eq. 4) the integral lower limit was $\log L_X = 41$ erg/s which corresponds to a lower limit of $\log L_B \simeq 35.5$ W for eq. 11 and, according to the R_X distribution and the relation between $L_{1.4}$ and L_K (eq. 7) to a lower limit of $\log L_K \simeq 34.5$ W for eq. 10. The resulting kinetic power density would be similar if, at all luminosities, the conversion of the radio into kinetic luminosity by Best et al. (2006), eq. 7, would be used, while a factor 4-6 lower values would be obtained using the relation from Willott et al. (1999), eq. 6, only. As shown in Figure 12 this difference is caused by the steep drop off of the 1.4 GHz radio LF at luminosities higher than $\log L_R \sim 25$ W (see Figure 9); as a consequence the resulting power density (the integrated kinetic LF) depends mainly on which conversion of the radio luminosity into kinetic power is used at low luminosities.

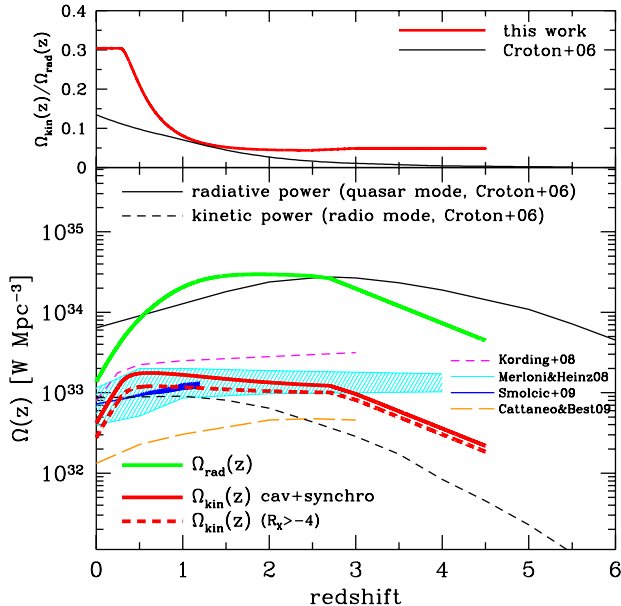


FIG. 14.— *Bottom*. Power density as a function of redshift. The kinetic power density derived from the best fit solution #5 is shown by a continuous red line. The red dashed line shows the result if the more radio loud objects ($R_X > -4$) only are used (see text and Figure 9). The magenta and orange dashed lines show the kinetic luminosity density as estimated by Kording et al. (2008) and Cattaneo & Best (2009), respectively. The cyan and blue areas show the estimates by Merloni & Heinz (2008) and Smolčić et al. (2010), respectively. The radiative and kinetic power densities, as used in the model of Croton et al. (2006), are shown by continuous and dashed black lines, respectively. *Top*. Ratio between the kinetic and radiative power densities. The red and black continuous lines are the results by our fit #5 and Croton et al. (2006), respectively.

5. DISCUSSION

The probability distribution function of R_X , $P(R_X|L_X, z)$ estimated in Section 3 depends on both luminosity and redshift: the average R_X increases with decreasing luminosity and (possibly) increasing redshift (see best fit #5 in Table 2 and Figure 6). The observed increase of the average R_X value with decreasing luminosity is similar to previous results and models where (in analogy with X-ray binaries) low luminosity AGN are expected to be more likely radio loud⁴ (see e.g. Merloni & Heinz 2008; KÖrding, Jester & Fender 2008).

The knowledge of the R_X distribution, once convolved with the X-ray LF and the relations between the kinetic and radio luminosity, allows to estimate the kinetic LF and its evolution. At luminosities higher than the break of the bolometric LF ($L_K \sim 10^{39}$ W) the kinetic LF results to be more than two orders of magnitude smaller than the bolometric LF (see Figure 12), while at lower luminosities the relevance of the kinetic LF increases, reaching values comparable to the bolometric one at $L_K \sim 10^{36}$ W, which

roughly corresponds to the minimum luminosity experimentally probed by the X-ray LF ($\log L_X \sim 42$ erg/s; see e.g. La Franca et al. 2005). The kinetic LF shows a maximum in the range $10^{35} < L_K < 10^{37}$ W, where most ($\sim 90\%$) of the kinetic power density (shown in Figure 13) is produced.

In Figure 14 we show the kinetic and radiative power density as a function of the redshift. We also show the kinetic power density corresponding to the more radio emitting AGN having R_X larger than -4 , and then corresponding to the population which is typically represented by the radio LF (see in Figure 9 the comparison of the reproduced radio LF with $R_X > -4$ with the radio LF of FRI sources as measured by Smolčić et al. 2009). It is then possible to see that the kinetic power density could be underestimated by up to a factor of about two, if the radio LF alone is used, without taking into account the low radio luminosity AGN population.

Our estimates are in qualitative agreement with the trends of the radiative and kinetic power density with redshift used by Croton et al (2006) at $z > 0.5$ (see Figure 14). However, at lower redshifts we find a sharp (a factor of five) decrease of both radiative and kinetic power densities from $z \sim 0.5$ (i.e. about 5 billion years ago) to $z = 0$. This result is quite robust, and comes from the strong negative evolution of the AGN LF from $z \sim 2$ down to $z = 0$, which has been observed since the first studies of the QSO evolution in the optical (see e.g. Marshall et al. 1983; Croom et al. 2009 for recent results), and measured by many other authors in the hard X-rays (e.g. Ueda et al. 2003; La Franca et al. 2005; Hasinger 2008). Conversely, Croton et al. (2006) assume an almost continuous increase of both the kinetic and radiative powers, due to the assumption that both phenomena are related to an almost constant accretion onto the SMBH. Under this assumption Croton et al. (2006) overestimate both the AGN radiative and kinetic power densities at low ($z \lesssim 0.5$) redshift, allowing only for a much shallower decrease of the kinetic feedback (a factor of 30%) and of the AGN radiative power.

In Figure 14 (*top*) we show the ratio of the $\Omega_K/\Omega_{\text{rad}}$ plotted as function of redshift. According to our best fit #5, at $z > 0.5$ the kinetic power density is $\sim 5\%$ of the radiative density, and increases up to about 30% at decreasing redshifts. This increase at low redshifts of the ratio of the kinetic power to the radiative power density could help in modeling the quenching of the star formation at low redshift. In Croton et al. (2006) a milder increase is assumed, which should be attributed to the, above discussed, overestimate of the low redshift AGN radiative density.

Many previous results on the AGN kinetic LF are based on the convolution of some relations between the kinetic and radio power with direct measures of the AGN radio LF (e.g. Shankar et al. 2008; Merloni & Heinz 2008; KÖrding, Jester & Fender 2008; Cattaneo & Best 2009; Smolčić et al. 2009). As already discussed in the introduction, the measure of the R_X distribution is useful in order to allow a detailed implementation of the AGN feedback within the galaxy formation and evolution models because it gives the opportunity to predict the radio luminosity (and thus feedback) of each AGN as a function of its luminosity (accretion rate) and redshift.

According to our best fit #5, in the redshift range

⁴ As discussed in sect. 2 and 3, these trends do not include the most luminous (radio loud; mostly FRII) sources. As far as the more radio loud population is concerned, it has been observed that the fraction of more radio loud AGN increases with increasing optical (or X-ray) luminosity and decreasing redshift (Miller et al. 1990; Visnovsky et al. 1992; Padovani 1993; La Franca et al. 1994; Goldschmidt et al. 1999; Ivezić et al. 2002; Cirasuolo et al. 2003; Jiang et al. 2007).

$0.5 < z < 3$ the integrated kinetic power density is $\sim 1-2 \times 10^{33} \text{ W Mpc}^{-3}$ (see Figure 14). This is in rough agreement with the previous estimates by Merloni & Heinz (2008), K rding, Jester and Fender (2008) and Smol ci c et al. (2009). At lower redshift ($z < 0.5$) we observe a drop by a factor of five, similar to what observed by K rding, Jester and Fender (2008), and in agreement, within the uncertainties, with Merloni & Heinz (2008). On the contrary our results are, at any redshift, 2-8 times greater than that reported by Cattaneo & Best (2009).

Merloni & Heinz (2008) found that their kinetic LF roughly corresponds to a constant overall efficiency in converting the accreted mass energy into kinetic power $\epsilon_{kin} \simeq 3 - 5 \times 10^{-3}$ (where $L_K = \epsilon_{kin} \dot{m} c^2$). Their results are similar to ours where, according to equations 10 and 11, on average, we have $\epsilon_{kin} \simeq (\Omega_K/\Omega_R) \epsilon_R \simeq 5 \times 10^{-3}$, as we measure $\Omega_K/\Omega_R \simeq 0.05$ (see the Ω_K/Ω_R ratio as a function of redshift in Figure 14, *top*), and assuming a radiative efficiency $\epsilon_R = 0.1$ (Marconi et al. 2004). However, we observe an increase of the Ω_K/Ω_R ratio (i.e. of the kinetic efficiency) up to a value 0.3 at decreasing redshifts, which Merloni & Heinz (2008) observe in the most massive objects only ($> 10^8 - 10^9 M_\odot$; see e.g. their Figure 13). It should also be noted that, although the integrated kinetic power density of Merloni & Heinz (2008) is in agreement with our estimate, their kinetic LF is similar to our measure only at $L_K \sim 10^{36} \text{ W}$ (see Figure 13), while it is definitely larger (by about an order of magnitude) at higher kinetic luminosities. Once integrated in luminosity, the computed power densities are similar (at $z \lesssim 3$) because our low luminosity limit ($L_K = 10^{34} \text{ W}$) is significantly lower than that used by Merloni & Heinz (2008; $L_K = 10^{36} \text{ W}$).

Shankar et al. (2008), found that the ratio of the kinetic to bolometric luminosity, defined as $g_k = L_K/L_B$, is constant and equal to $g_k = 0.10$ with a scatter of $\sigma = 0.38$. According to equations 10 and 11, g_k corresponds roughly to the ratio Ω_K/Ω_{rad} (plotted as function of redshift in Figure 14, *top*), which, as discussed above, levels at ~ 0.05 at $z > 1$ while increases up to 0.3 at $z = 0$.

6. CONCLUSIONS

We used a sample of more than 1600 X-ray selected AGN observed at 1.4 GHz to measure the probability distribution function, $P(R_X|L_X, z)$, of the ratio R_X of the radio to intrinsic X-ray luminosity, as a function of the X-ray luminosity and redshift.

The knowledge of the $P(R_X|L_X, z)$ distribution is necessary to estimate the AGN kinetic (radio) feedback into the hosting galaxies by allowing to couple it with the luminous, accreting, phases of the AGN activity.

The average value of R_X increases with decreasing X-ray luminosities and (possibly) increasing redshift. At variance, we did not find a statistical significant difference between the radio properties of the X-ray absorbed ($N_H > 10^{22} \text{ cm}^{-2}$) and un-absorbed AGN.

We were able to better measure the densities of the more radio quiet ($R_X < -4$) AGN which resulted to be responsible of about half of the derived kinetic power density.

According to our analysis the value of the kinetic energy density is in qualitative agreement with the last generation galaxy evolution scenarios, where radio mode

AGN feedback is invoked to quench the star formation in galaxies and slow down the cooling flows in galaxy clusters. However at redshifts below 0.5, similarly to what observed by K rding, Jester and Fender (2008), we find a sharp (about a factor of five) decrease of the kinetic energy density, which is strictly related the AGN density evolution, but which is not included in many of the galaxy/AGN formation and evolution models where, instead, the radio mode feedback is assumed to continuously increase (or only smoothly decrease) at low redshift.

We thank A. Lamastra, N. Menci, R. Morganti, P. Ranalli, V. Smol ci c and G. Zamorani for discussions. We are grateful to L. Trouille and A. Barger for the support in allowing us to use the CLANS data, and to D. Ballantyne, R. Della Ceca and A. Merloni for providing data in machine readable format. We thanks the anonymous referee for his useful comments. We acknowledge financial contribution from contract ASI-INAF I/088/06/0 and PRIN-MIUR grant 2006-02-5203.

REFERENCES

- Akiyama, M., et al. 2000, *ApJ*, 532, 700
- Akiyama, M., Ueda, Y., Ohta, K., Takahashi, T., & Yamada, T. 2003, *ApJS*, 148, 275
- Alexander, D. M., et al. 2003, *AJ*, 126, 539
- Ballantyne, D. R. 2009, *ApJ*, 698, 1033
- Barcons, X., et al. 2007, *A&A*, 476, 1191
- Barnes, J. E., & Hernquist, L. 1992, *ARA&A*, 30, 705
- Becker, R. H., White, R. L., & Helfand, D. J. 1995, *ApJ*, 450, 559
- Beckmann, V., Soldi, S., Shrader, C. R., Gehrels, N., & Produit, N. 2006, *ApJ*, 652, 126
- Best, P. N., Kaiser, C. R., Heckman, T. M., & Kauffmann, G. 2006, *MNRAS*, 368, L67
- Biggs, A. D., & Ivison, R. J. 2006, *MNRAS*, 371, 963
- Birzan, L., Rafferty, D. A., McNamara, B. R., Wise, M. W., & Nulsen, P. E. J. 2004, *ApJ*, 607, 800
- Birzan, L., McNamara, B. R., Nulsen, P. E. J., Carilli, C. L., & Wise, M. W. 2008, *ApJ*, 686, 859
- Bondi, M., Ciliegi, P., Schinnerer, E., Smolčić, V., Jahnke, K., Carilli, C., & Zamorani, G. 2008, *ApJ*, 681, 1129
- Bower, R. G., Benson, A. J., Malbon, R., Helly, J. C., Frenk, C. S., Baugh, C. M., Cole, S., & Lacey, C. G. 2006, *MNRAS*, 370, 645
- Brinkmann, W., Laurent-Muehleisen, S. A., Voges, W., Siebert, J., Becker, R. H., Brotherton, M. S., White, R. L., & Gregg, M. D. 2000, *A&A*, 356, 445
- Brunner, H., Cappelluti, N., Hasinger, G., Barcons, X., Fabian, A. C., Mainieri, V., & Szokoly, G. 2008, *A&A*, 479, 283
- Brusa, M., et al. 2009a, *ApJ*, 693, 8
- Brusa, M., et al. 2009b, *A&A*, 507, 1277
- Brusadin, V., 2003, Degree Thesis, University Roma Tre
- Cappelluti, N., et al. 2009, *A&A*, 497, 635
- Cattaneo, A., Dekel, A., Devriendt, J., Guiderdoni, B., & Blaizot, J. 2006, *MNRAS*, 370, 1651
- Cattaneo, A., & Best, P. N. 2009, *MNRAS*, 395, 518
- Cavaliere, A., & Vittorini, V. 2000, *ApJ*, 543, 599
- Ciliegi, P., Zamorani, G., Hasinger, G., Lehmann, I., Szokoly, G., & Wilson, G. 2003, *A&A*, 398, 901
- Cirasuolo, M., Celotti, A., Magliocchetti, M., & Danese, L. 2003, *MNRAS*, 346, 447
- Cocchia, F., et al. 2007, *A&A*, 466, 31
- Condon, J. J., Cotton, W. D., Greisen, E. W., Yin, Q. F., Perley, R. A., Taylor, G. B., & Broderick, J. J. 1998, *AJ*, 115, 1693
- Croom, S. M., et al. 2009, *MNRAS*, 399, 1755
- Croton, D. J., et al. 2006, *MNRAS*, 365, 11
- Della Ceca, R., et al. 2004, *A&A*, 428, 383
- Di Matteo, T., Springel, V., & Hernquist, L. 2005, *Nature*, 433, 604
- Elbaz, D., et al. 2007, *A&A*, 468, 33
- Fabian, A. C. 1999, *MNRAS*, 308, L39
- Fanaroff, B. L., & Riley, J. M. 1974, *MNRAS*, 167, 31P
- Feruglio, C. et al. 2008, *A&A*, 488, 417
- Fiore, F., et al. 2003, *A&A*, 409, 79
- Goldschmidt, P., Kukula, M. J., Miller, L., & Dunlop, J. S. 1999, *ApJ*, 511, 612
- Granato, G. L., De Zotti, G., Silva, L., Bressan, A., & Danese, L. 2004, *ApJ*, 600, 580
- Grossan, B. A. 1992, Ph.D. Thesis,
- Hasinger, G. 2008, *A&A*, 490, 905
- Heinz, S., Merloni, A., & Schwab, J. 2007, *ApJ*, 658, L9
- Hopkins, P. F., Hernquist, L., Cox, T. J., Di Matteo, T., Martini, P., Robertson, B., & Springel, V. 2005, *ApJ*, 630, 705
- Hopkins, P. F., Hernquist, L., Cox, T. J., Di Matteo, T., Robertson, B., & Springel, V. 2006, *ApJS*, 163, 1
- Ilbert, O., et al. 2009, *ApJ*, 690, 1236
- Ivezić, Ž., et al. 2002, *AJ*, 124, 2364
- Jarvis, M. J., & Rawlings, S. 2004, *New Astronomy Review*, 48, 1173
- Jiang, L., Fan, X., Ivezić, Ž., Richards, G. T., Schneider, D. P., Strauss, M. A., & Kelly, B. C. 2007, *ApJ*, 656, 680
- Kauffmann, G., & Haehnelt, M. 2000, *MNRAS*, 311, 576
- Körding, E. G., Jester, S., & Fender, R. 2008, *MNRAS*, 383, 277
- Krause, M., & Gaibler, V. 2009, *arXiv:0906.2122*
- La Franca, F., Gregorini, L., Cristiani, S., de Ruiter, H., & Owen, F. 1994, *AJ*, 108, 1548
- La Franca, F., Franceschini, A., Cristiani, S., & Vio, R. 1995, *A&A*, 299, 19
- La Franca, F., & Cristiani, S. 1997, *AJ*, 113, 1517
- La Franca, F., et al. 2002, *ApJ*, 570, 100
- La Franca, F., et al. 2005, *ApJ*, 635, 864
- Hampton, M., Margon, B., & Bowyer, S. 1976, *ApJ*, 208, 177
- Li, Z.-Y., Wu, X.-B., & Wang, R. 2008, *ApJ*, 688, 826
- Marconi, A., Risaliti, G., Gilli, R., Hunt, L. K., Maiolino, R., & Salvati, M. 2004, *MNRAS*, 351, 169
- Marshall, H. L., Tananbaum, H., Avni, Y., & Zamorani, G. 1983, *ApJ*, 269, 35
- Marulli, F., Bonoli, S., Branchini, E., Moscardini, L., & Springel, V. 2008, *MNRAS*, 385, 1846
- Mauch, T., Murphy, T., Buttery, H. J., Curran, J., Hunstead, R. W., Piestrzynski, B., Robertson, J. G., & Sadler, E. M. 2003, *MNRAS*, 342, 1117
- McNamara, B. R., et al. 2000, *ApJ*, 534, L135
- Menci, N., Fontana, A., Giallongo, E., Grazian, A., & Salimbeni, S. 2006, *ApJ*, 647, 753
- Menci, N., Fiore, F., Puccetti, S., & Cavaliere, A. 2008, *ApJ*, 686, 219
- Merloni, A., Heinz, S., & di Matteo, T. 2003, *MNRAS*, 345, 1057
- Merloni, A., & Heinz, S. 2007, *MNRAS*, 381, 589
- Merloni, A., & Heinz, S. 2008, *MNRAS*, 388, 1011
- Middelberg, E., et al. 2008, *AJ*, 135, 1276
- Miller, L., Peacock, J. A., & Mead, A. R. G. 1990, *MNRAS*, 244, 207
- Miller, N. A., Fomalont, E. B., Kellermann, K. I., Mainieri, V., Norman, C., Padovani, P., Rosati, P., & Tozzi, P. 2008, *ApJS*, 179, 114
- Monaco, P., Salucci, P., & Danese, L. 2000, *MNRAS*, 311, 279
- Noeske, K. G., et al. 2007, *ApJ*, 660, L43
- Owen, F. N., & Morrison, G. E. 2008, *AJ*, 136, 1889
- Padovani, P. 1993, *MNRAS*, 263, 461
- Padovani, P., Mainieri, V., Tozzi, P., Kellermann, K. I., Fomalont, E. B., Miller, N., Rosati, P., & Shaver, P. 2009, *ApJ*, 694, 235
- Panessa, F., Barcons, X., Bassani, L., Cappi, M., Carrera, F. J., Ho, L. C., & Pellegrini, S. 2007, *A&A*, 467, 519
- Puccetti, S. et al. 2006, *A&A*, 457, 501
- Ranalli, P., Comastri, A., & Setti, G. 2003, *A&A*, 399, 39
- Richards, E. A. 2000, *ApJ*, 533, 611
- Sacchi, N., et al. 2009, *ApJ*, 703, 1778
- Salvato, M., et al. 2009, *ApJ*, 690, 1250
- Saxton, C. J., Bicknell, G. V., Sutherland, R. S., & Midgley, S. 2005, *MNRAS*, 359, 781
- Sazonov, S., Revnivtsev, M., Krivonos, R., Churazov, E., & Sunyaev, R. 2007, *A&A*, 462, 57
- Schinnerer, E., et al. 2007, *ApJS*, 172, 46
- Seymour, N., et al. 2008, *MNRAS*, 386, 1695
- Shabala, S., & Alexander, P. 2009, *ApJ*, 699, 525
- Shankar, F., Cavaliere, A., Cirasuolo, M., & Maraschi, L. 2008, *ApJ*, 676, 131
- Silk, J., & Rees, M. J. 1998, *A&A*, 331, L1
- Smolčić, V., et al. 2009, *ApJ*, 696, 24
- Smolčić, V., et al. 2010, *ApJ*, 708, 909
- Springel, V. 2005, *MNRAS*, 364, 1105
- Sutherland, W., & Saunders, W. 1992, *MNRAS*, 259, 413
- Sutherland, R. S., & Bicknell, G. V. 2007, *ApJS*, 173, 37
- Tortora, C., Antonuccio-Delogu, V., Kaviraj, S., Silk, J., Romeo, A. D., & Becciani, U. 2009, *MNRAS*, 396, 61
- Tozzi, P., et al. 2009, *ApJ*, 698, 740
- Trouille, L., Barger, A. J., Cowie, L. L., Yang, Y., & Mushotzky, R. F. 2008, *ApJS*, 179, 1
- Trump, J. R., et al. 2009, *ApJ*, 696, 1195
- Tueller, J., Mushotzky, R. F., Barthelmy, S., Cannizzo, J. K., Gehrels, N., Markwardt, C. B., Skinner, G. K., & Winter, L. M. 2008, *ApJ*, 681, 113
- Ueda, Y., et al. 1999, *ApJ*, 518, 656
- Ueda, Y., Akiyama, M., Ohta, K., & Miyaji, T. 2003, *ApJ*, 598, 886
- Vasudevan, R. V., & Fabian, A. C. 2009, *MNRAS*, 392, 1124
- Visnovsky, K. L., Impey, C. D., Foltz, C. B., Hewett, P. C., Weymann, R. J., & Morris, S. L. 1992, *ApJ*, 391, 560
- Volonteri, M., Haardt, F., & Madau, P. 2003, *ApJ*, 582, 559
- White, R. L., Becker, R. H., Helfand, D. J., & Gregg, M. D. 1997, *ApJ*, 475, 479
- Willott, C. J., Rawlings, S., Blundell, K. M., & Lacy, M. 1999, *MNRAS*, 309, 1017
- Wilman, R. J., et al. 2008, *MNRAS*, 388, 1335